Low threshold current single-cell hexapole mode photonic crystal laser

Min-Kyo Seo,[a] Kwang-Yong Jeong, Jin-Kyu Yang, and Yong-Hee Lee
Department of Physics, Korea Advanced Institute of Science and Technology, Daejeon 305-701, Korea

Hong-Gyu Park
Department of Chemistry and Chemical Biology, Harvard University, Cambridge, Massachusetts 02138

Sung-Bock Kim
Telecommunication Basic Research Laboratory, Electronics and Telecommunications Research Institute, Daejeon 305-600, Korea

(Received 18 March 2007; accepted 3 April 2007; published online 27 April 2007)

The authors report an electrically driven, hexapole mode, single-cell photonic crystal laser operating at 1537.8 nm. Electrical current is supplied through a submicrometer-sized current post beneath the cavity center. This wavelength-scale single-cell photonic crystal laser operates in a single mode with threshold current of ~100 μA at room temperature. Operation in the hexapole mode is confirmed by the near-field profile, far-field polarization, and the finite-difference time-domain computation based on the fabricated cavity structure. © *2007 American Institute of Physics*.
[DOI: 10.1063/1.2734391]

Recently, various wavelength-scale photonic crystal (PhC) lasers have been demonstrated.[1–3] The resonant mode of the PhC cavity could have a high quality (Q) factor and very small mode volume simultaneously and thus offers potential as a platform for quantum optical photon sources.[4–9] The previous electrically driven, single mode, single-cell PhC laser was reported to operate in the monopole mode.[3] The photons coming out of the monopole mode, however, are highly diverging and cannot be easily collected with high efficiency. In comparison, the hexapole mode is known to have a Q factor over 10^6, much larger than that of the monopole mode.[10–12] Moreover, through simple modification, the output of the hexapole mode can be collected with high efficiency.[11] Thus, we believe that the hexapole mode is one of the realistic candidates for the efficient single photon source. In this letter, we report an electrically driven single-cell PhC laser with a low threshold current of 100 μA at room temperature. We confirm that the laser does operate in the hexapole mode through a contour finite-difference time-domain (FDTD) calculation based on the scanning electron microscope (SEM) image of the fabricated single-cell PhC cavity.

The schematic and SEM images of the electrically driven PhC laser are shown in Fig. 1. Six InGaAsP multiple quantum wells (MQWs) are placed in the middle of the slab of thickness of 282.5 nm. Doping densities of the top Si-doped n-layer and the bottom Zn-doped p-layer are $\sim 2.7 \times 10^{19}$ and $\sim 2.5 \times 10^{18}$ cm^{-3}, respectively. The sacrificial topmost InP layer is wet etched by diluted HCl solution ($HCl:H_2O=2:1$). The submicrometer-sized current post is formed by cold HCl wet-etching processes. This current post has to be small enough not to spoil the Q factor of the resonator too much but still large enough to supply holes smoothly. We succeed to control and reduce the post size gradually by increasing the wet-etching temperature from 10 °C to room temperature, as shown in Fig. 1(c).

For efficient current injection, the doping density of the n-doped top layer is also important. When the doping density is too low, a broad depletion region is formed in the proximity of photonic crystal air holes and available electron paths become narrow. The electrons, which have to travel a few microns from the top electrode, suffer from a resultant high electrical resistance.

Generally, a triangular lattice single-cell PhC cavity supports four possible modes: monopole, quadrupole, hexapole, and dipole modes.[13] Note that the hexapole and monopole

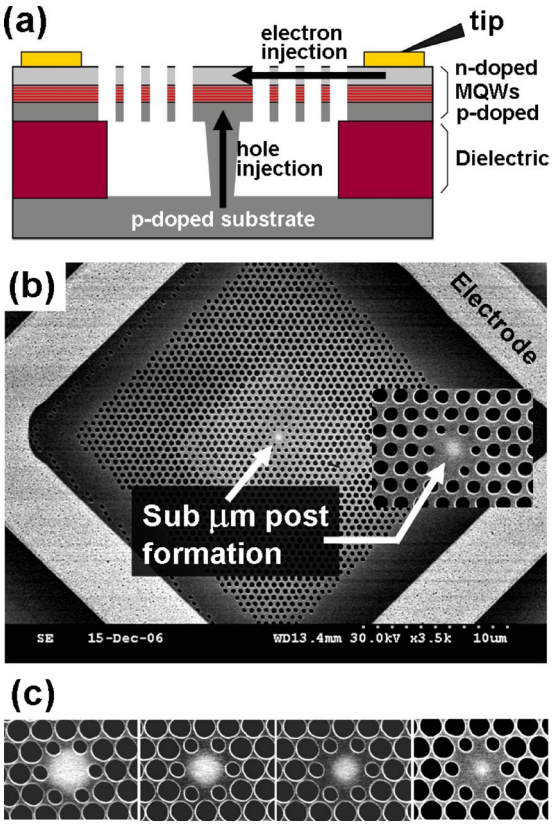

FIG. 1. (Color online) (a) Schematic diagram and (b) SEM image of the electrically driven single-cell PhC laser. At the center of the cavity, the white shadow image of the submicrometer-sized current post is shown. (c) Formation of the current post by phasing up the HCl wet-etching temperature.

[a]Electronic mail: b612@kaist.ac.kr

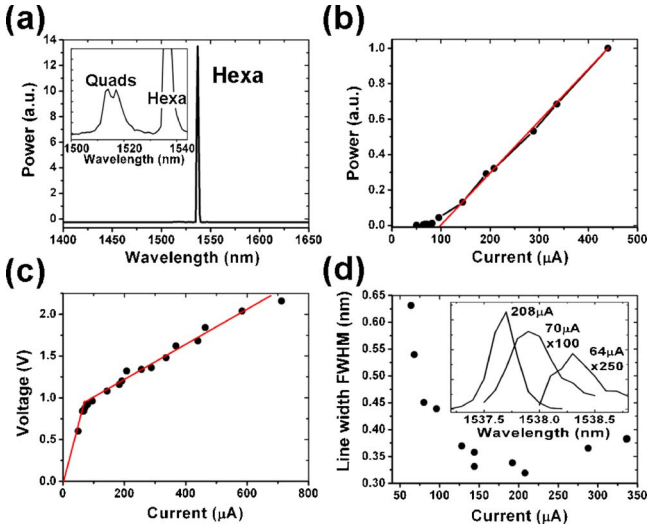

FIG. 2. (Color online) (a) Lasing spectrum measured at 450 μA. In the inset, two nonlasing quadrupole modes are observed, when the slit width of the spectrometer becomes five times broader. (b) Measured *L-I* curve of the hexapole mode laser. Threshold current is ~100 μA. (c) Typical electrical characteristics of the semiconductor laser. (d) Plot of the measured linewidth of the hexapole mode with different injected currents. In the inset, three selected spectra are shown.

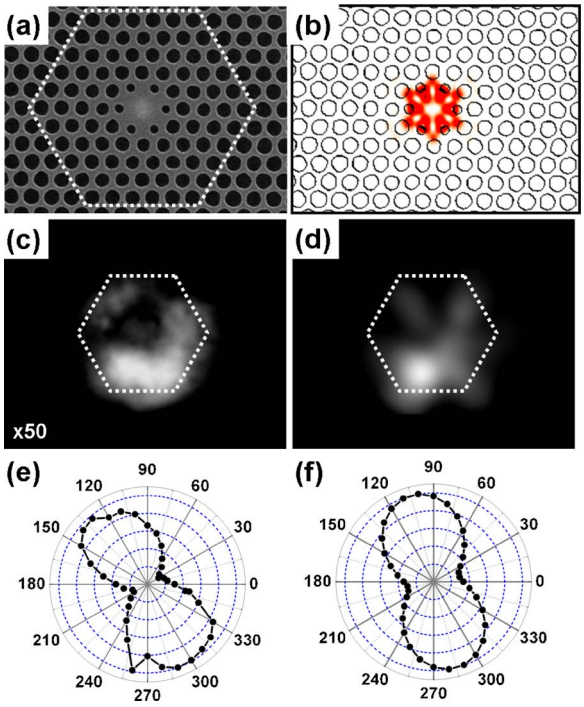

FIG. 3. (Color online) (a) SEM image of the single-cell hexapole mode PhC laser. (b) Electric field intensity profile of the hexapole mode from the contour FDTD calculation. The superimposed contour, employed in the calculation, is transformed from the SEM image. (c) Near-field image of the laser mode through an IR camera and 50× optical microscope lens. The white hexagon corresponds to that in (a). (d) The vertical component of the Poynting vector of the hexapole mode from the contour FDTD calculation. The profile, with consideration of the blurring effect by the objective lens, is captured at a vertical position of 1.5 μm above the PhC slab. [(e) and (f)] Far-field polarizations from the experiment and the contour FDTD calculation.

modes have zero photon density at the center of the cavity. We confirm that the Q factors of these modes are not affected appreciably even after the introduction of the central post if the size of the post is small enough. Among these two modes, the area of low photon density is larger for the hexapole mode than the monopole mode. Therefore, the hexapole mode more readily allows the larger central post that is to be used as a current path. On the other hand, the Q factors of the quadrupole and dipole modes are dramatically degraded with the central post located at the antinode site.

The PhC lattice constant of the fabricated structure is ~450 nm. The radii of PhC air holes and the nearest air holes are $0.37a$ and $0.20a$, respectively, where a is the lattice constant. The size on a side of the diamondlike current post is controlled down to $0.8a$. Typically, the post size estimated from the bare SEM image turns out to be about 10% smaller than the actual size. In our designed single-cell cavity, the hexapole mode and two doubly degenerated quadrupole modes are located within the electroluminescence spectrum centered near 1550 nm, with a spectral width of ~100 nm.

The fabricated single-cell PhC laser is pumped with 10 ns current pulses at an interval of 250 ns at room temperature. To minimize electrical noise and feedback, the electric pulses are supplied through an impedance-matched small copper plate connected to a bayonet-type connection cable. The peak injection current is measured by a fast oscilloscope. Through a 20× long-focal-length microscope objective lens, the output laser light is directed into the spectrometer.

Single mode lasing action is observed at 1537.8 nm with a threshold current of ~100 μA, as shown in Figs. 2(a) and 2(b). The electrical characteristics of the single-cell PhC laser, plotted by the peak voltage and the peak current value, are shown in Fig. 2(c). The turn-on voltage and electrical resistance are 0.9 V and 2.1 kΩ, respectively. Near the laser threshold, the pronounced linewidth narrowing is observed down to our spectral resolution of 0.3 nm, as shown in Fig. 2(d). As the current is further increased to over ~150 μA, we observe a plateau, followed by a slight broadening. We note that the nonequilibrium carrier dynamics appearing in microcavities with high spontaneous emission factor (β) at room temperature could be responsible for this behavior.[14] Furthermore, linewidth enhancement in the semiconductor laser due to the gain-refractive index coupling is reported.[15] The inset of Fig. 2(d) shows spectra taken at various pumping currents. Taking the spectral linewidth near the transparency current of 70 μA, the Q factor of the cold cavity for the hexapole mode is estimated to be ~3400.

The hexapole mode operation is confirmed by comparing the experimental measurements with the result obtained from the three-dimensional contour FDTD using data taken directly from the SEM image of the PhC cavity, as shown Figs. 3(a) and 3(b). Note that the contour FDTD method, which faithfully describes the actual structure, produces results that agree well with the experimental measurements. In the computation, a diamondlike current post of size of $0.8a$ on a side is used. The resonance wavelength depends very slightly on the size of the post. The computed resonance wavelength and the Q factor of the hexapole mode are 1540.1 nm and 6700, respectively. These values compare well with the experimentally measured values. The estimated mode volume is $0.80\ (\lambda/n)^3$ and the Purcell factor is about 630. Here, λ and n denote the resonant wavelength and refractive index (3.4) of the InGaAsP semiconductor slab, respectively. Note that the Purcell factor represents the maximum spontaneous emission rate enhancement of the "ideal" emitter-cavity coupling system in the weak coupling

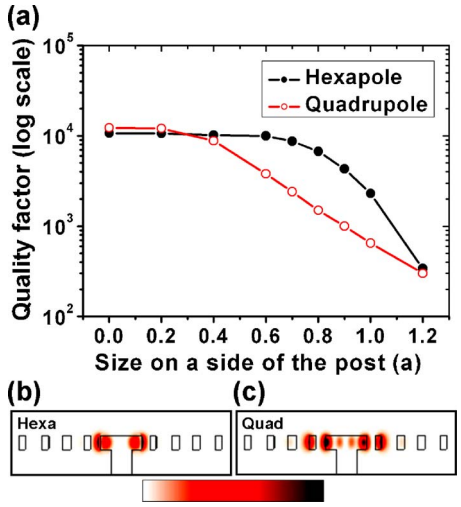

FIG. 4. (Color online) (a) Plot of the Q factors, from the contour FDTD calculation, of the hexapole and quadrupole modes with different central post side sizes. [(b) and (c)] Calculated electric field intensity profiles of the hexapole and quadrupole modes in the cross section.

regime.[4,5] The emission rate enhancement of a practical quantum dot (QD) within a semiconductor microcavity is limited by several parameters such as the position, polarization matching, and spectral detuning of the QD with respect to the cavity mode.[5,7,9]

An above-threshold image of the single-cell PhC resonator, captured by a 50× optical microscope lens, is shown in Fig. 3(c). Although the sixfold symmetry is broken in this near-field profile, the central intensity minimum, a signature of the hexapole mode, is still observable. We attribute this broken symmetry to the imperfectly fabricated nearest air holes and the central post. Observe that the vertical components of the propagating Poynting vectors at a plane 1.5 μm above the slab agree reasonably with the measured near-field profile, as shown in Fig. 3(d). Ideally, the far-field radiation of the ideal hexapole mode is unpolarized, owing to the well-balanced inner symmetry of the mode. However, in the real hexapole mode, the symmetry is easily perturbed and the vertical radiation becomes polarized, as shown in Fig. 3(e). We compare this measurement with the result of our contour FDTD computation shown in Fig. 3(f). It is also worth emphasizing that, by modifying the two nearest air holes on the x axis, linearly polarized vertical beaming can be obtained with high efficiency.[11] Efficient photon collection is one of the critical features for a practical single photon source.

Two quadrupole modes near 1514 and 1517 nm shown in the inset of Fig. 2 (1512 and 1519 nm in the contour FDTD calculation) are not clearly resolved because of the low Q values of the modes. In fact, in order to detect the very weak quadrupole peaks, the input slit width of the spectrometer can be increased at the expense of resolution. The effect of the central post is summarized in Fig. 4 by the contour FDTD calculation. Note that the Q factor of the hexapole is reduced only slightly with the introduction of the central post. This is due to the negligible photon density above the central post. On the other hand, the cavity loss of the quadrupole mode increases by nearly an order of magnitude because of the high photon density at the center and unavoidable losses through the central post, as shown in Fig. 4(c). In fact, the central current post, with its size on a side of $0.6-1.0a$, promotes the single hexapole mode lasing and suppresses the onset of lasing in the quadrupole mode.

In summary, the electrically driven single-cell PhC laser operating in the hexapole mode is demonstrated at room temperature. This wavelength-scale PhC laser works in a single mode with threshold current of ~100 μA. A submicrometer post is introduced for efficient carrier injection and this small post also functions as a mode selector. Operation of the hexapole mode is confirmed through the near-field image, polarization, and contour FDTD calculation. We believe that this electrically driven PhC hexapole mode cavity will be an ideal platform for practical single photon sources for quantum information.

One of authors (M.K.S.) would like to thank Soon-Hong Kwon in Germany and Se-Heon Kim. This work was supported by the Korea Science and Engineering Foundation (KOSEF) (No. ROA-2006-000-10236-0) and the Korea Foundation for International Cooperation of Science and Technology (KICOS) (No. M60605000007-06A0500-00710) through grants provided by the Korean Ministry of Science and Technology (MOST).

[1] O. Painter, R. K. Lee, A. Scherer, A. Yariv, J. D. O'Brien, P. D. Dapkus, and I. Kim, Science **284**, 1819 (1999).
[2] S. Strauf, K. Hennessy, M. T. Rakher, Y. S. Choi, A. Badolato, L. C. Andreani, E. L. Hu, P. M. Petroff, and D. Bouwmeetster, Phys. Rev. Lett. **96**, 127404 (2006).
[3] H.-G. Park, S.-H. Kim, S.-H. Kwon, Y.-G. Ju, J.-K. Yang, J.-H. Baek, S.-B. Kim, and Y.-H. Lee, Science **305**, 1444 (2004); H.-G. Park, S.-H. Kim, M.-K. Seo, Y.-G. Ju, S.-B. Kim, and Y.-H. Lee, IEEE J. Quantum Electron. **41**, 1131 (2005).
[4] K. J. Vahala, Nature (London) **424**, 839 (2003).
[5] J. M. Gérard and B. Gayral, Proc. SPIE **5361**, 88 (2004).
[6] E. Knill, E. Laflamme, and G. J. Milburn, Nature (London) **409**, 46 (2001).
[7] D. Englund, D. Fattal, E. Waks, G. Solomon, B. Zhang, T. Nakaoka, Y. Arakawa, Y. Yamamoto, and J. Vučković, Phys. Rev. Lett. **95**, 013904 (2005).
[8] T. Yoshie, A. Scherer, J. Hendrickson, G. Khitrova, H. M. Gibbs, G. Rupper, C. Ell, O. B. Shchekin, and D. G. Deppe, Nature (London) **432**, 200 (2004).
[9] A. Badolato, K. Hennessy, M. Atatüre, J. Dreiser, E. L. Hu, P. M. Petroff, and A. Imamoglu, Science **308**, 1158 (2005).
[10] H.-Y. Ryu, M. Notomi, and Y.-H. Lee, Appl. Phys. Lett. **83**, 4294 (2003).
[11] S.-H. Kim, S.-K. Kim, and Y.-H. Lee, Phys. Rev. B **73**, 235117 (2006).
[12] S.-K. Kim, G.-H. Kim, S.-H. Kim, Y.-H. Lee, S.-B. Kim, and I. Kim, Appl. Phys. Lett. **88**, 161119 (2006).
[13] H.-G. Park, J.-K. Hwang, J. Huh, H.-Y. Ryu, S.-H. Kim, J.-S. Kim, and Y.-H. Lee, IEEE J. Quantum Electron. **38**, 1353 (2002).
[14] U. Mohideen, R. E. Slusher, F. Jahnke, and S. W. Koch, Phys. Rev. Lett. **73**, 1785 (1994).
[15] G. Björk, A. Karlsson, and Y. Yamamoto, Appl. Phys. Lett. **60**, 304 (1992).